Chemical compositions and plasma parameters of planetary nebulae with Wolf-Rayet type central stars ⋆

P.Girard[1,2], J.Köppen[2,3,4], and A.Acker[2]

[1] Observatoire Aquitain des Sciences de l'Univers, L3AB, 2 rue de l'Observatoire, BP 89, 33270 Floirac, France
[2] Observatoire Astronomique de Strasbourg, 11 rue de l'Université, 67000 Strasbourg, France
[3] Institut für Theoretische Physik und Astrophysik, Universität Kiel, D-24098 Kiel, Germany
[4] International Space University, Parc d'Innovation, F-67400 Illkirch, France

Received / accepted

Abstract. Chemical compositions and other properties of planetary nebulae around central stars of spectral types [WC], [WO], and *wels* are compared with those of "normal" central stars, in order to clarify the evolutionary status of each type and their interrelation. We use plasma diagnostics to derive from optical spectra the plasma parameters and chemical compositions of 48 WR planetary nebulae. We also reanalyze the published spectra of a sample of 167 non-WR PN. The results as well as the observational data are compared in detail with those from other studies of the objects in common. We confirm that [WC], [WO] and *wels* nebulae are very similar to those "normal" PN: the relation between [N II] and [O III] electron temperatures, abundances of He, N, O, Ne, S and Ar, and the number of ionizing photons show no significant differences. They also share very similar infrared (IRAS, DENIS) properties. The central star's spectral type is clearly correlated with electron density, temperature and excitation class of the nebula, [WC] nebulae tend to be smaller than the other types. All this corroborates the view of an evolutionary sequence from cool [WC 11] central stars inside dense, low excitation nebulae towards hot [WO 1] stars with low density, high excitation nebulae. The *wels* PN, however, appear to be a separate class of objects, not linked to WRPN by evolution: nebular excitation, electron temperature and density, and the number of ionizing photons all cover the whole range found in the other types. Their lower mean N/O ratio and slightly lower He/H suggest progenitor stars less massive than for the other PN types. Furthermore, the differences between results of different works are dominated by the differences in observational data rather than differences in the analysis methods.

Key words. planetary nebulae: abundances – stars: abundances – stars: evolution – stars: Wolf-Rayet – ISM: planetary nebulae – stars: AGB

1. Introduction

Planetary nebulae (PN) are the highly visible transitionary phase in the life of intermediate mass stars on their evolution from the asymptotic giant branch to their final destination, the white dwarfs. Among the 1300 objects known in our Milky Way (Acker et al. 1992, 1996b), there are about 6% whose central stars show broad emission lines, characteristic of the [WR] spectral type, and most likely produced by a massive continuous mass loss from the central star. Whether these objects form a group or an evolutionary phase or evolutionary sequence distinctly different from the other, "normal" PN, is still not fully understood.

That PN with [WR] central stars do not seem to have very much different properties than normal, non-WR objects was shown by Górny & Stasińska (1995) who found that bipolar nebulae constitute about 20 % of the total in both WR and non-WR objects. Also, the distribution of He/H, N/O and C/O abundance ratios are the same in either group. Both aspects indicate that the WR phenomenon does not preferentially occur in more massive central stars, hence more massive progenitor stars. Acker et al. (1996a), Górny & Tylenda (2000) and Peña et al. (2001) showed that the majority of [WR] PN seems to form an evolutionary sequence from late-type [WC] inside high-density nebulae to early-type [WO] with low-density nebulae.

In their recent quantitative classification of central stars, Acker & Neiner (2003) distinguish two sequences from the late-type [WC] to the early-type [WO]: The spectra of hot [WO 1...4] types are dominated by the highly

Send offprint requests to: girard@obs.u-bordeaux1.fr

⋆ Based on observations obtained at the European Southern Observatory (ESO), La Silla, Chile

ionised oxygen lines, while those of the cooler [WC 4...11] types are marked by carbon lines. There seems to be an evolutionary sequence from [WC 11] to [WO 1]. The *wels* (weak emission line stars) objects differ from other central stars (Tylenda, Acker & Stenholm 1993) and are not part in this classification scheme.

More recently, Górny et al. (2004) found that the proportion of WRPN in the Galactic bulge is about 15%, significantly larger than in the disk (about 6%). Among the bulge WRPN about 47% are of type later than [WC 9]. In the disk this fraction amounts to only 17%. However, this finding is strongly sensitive to observational selection effects. They confirm the strong trend for the density to decrease towards late-type [WC]. Oxygen abundances in bulge WRPN are found to be the same as in the bulge non-WR, and the N/O distributions of PN in disk, bulge and of [WR] type are similar.

Another age indicator is the dust temperature derived from near and mid infrared data, indicating an evolutionary sequence from carbon AGB stars to [WC] PNe (Acker et al. 1996a). Gòrny et al. (2001) found that a sizeable fraction of WRPN seems to contain hot dust (1000-2000 K), probably in the winds of the central stars. The mean dust temperature decreases towards late-type [WC], in line with an evolutionary sequence from [WC11] to [WC2] ([WO2]).

The present paper presents the study of a homogeneous sample of nebulae around [WR] nuclei, using the high S/N spectra which had been used to study the [WR] central stars by Acker & Neiner (2003). These objects constitute a sample different from that of Peña et al. (2001), and it seems interesting to confirm (or not) the conclusions of these authors as well as those by Górny et al. (2004).

After presenting the observational material in section 2 and describing the analysis of the spectra in section 3, we study the chemical compositions of the various types of nebulae in section 4. We also compare the different groups with respect to other global relations in section 5, investigate the relation between central stars and the nebulae (section 6), and analyse the infrared properties (section 7). In appendices 8 and 9 we study the influences on the abundances due to differences in observational data and analysis methods.

2. Observational material

90 spectra of PN around central stars with emission lines were obtained in March 1994, July 1994, and July 1995 with the Boller & Chivens spectrograph and the CCD detector on the 1.52m telescope at ESO, Chile. The wavelength range is from 3700 Å to 7500 Å, with a spectral resolution of 1500 (more details can be found in Acker & Neiner 2003). Exposure times of 40 min and 5 min were employed, giving signal to noise ratios of better than 30 for most objects. For the analyses, the 48 objects with the best spectra were selected.

The quality of the data and their reduction can be assessed by looking at the line ratio of the [O III] 5007 and 4959 Å doublet which is independent of physical conditions in the nebula. Figure 1 shows that in all objects values very close to 3.0 are found, but slightly above the theoretical value from Mendoza (1983), as expected (cf. Acker et al. 1989). Only a few objects with faint spectra exhibit somewhat larger deviations.

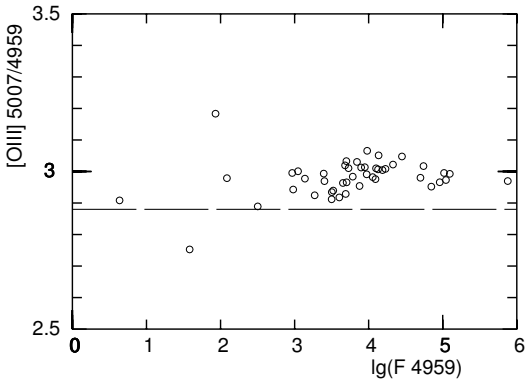

Fig. 1. The intensity ratio of the [O III] 5007 and 4959 Å lines as a function of the flux (arbitrary units) in the 4959 Å line. The horizontal line indicates the value exspected from the atomic data compiled by Mendoza (1983)

Another check is provided by the intensity ratios of the de-reddened He I lines at 5876, 4471, and 6678 Å which are not very sensitive to nebular conditions. All 33 objects which contain the three lines are found within 20 percent of the theoretical values (Fig. 2).

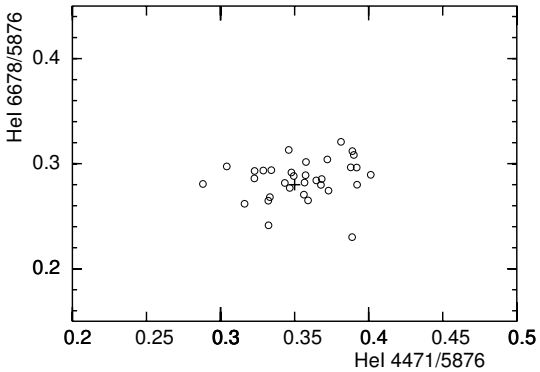

Fig. 2. The intensity ratios of the HeI 5876, 4471, and 6678 Å lines. The plus sign marks the low density value for $T_e = 10^4$ K.

Since a number of the objects have been observed by other authors, we compared our data in detail with previous measurements. The He II 4686Å line covers a large

range in values among the objects. As shown by Fig. 3, our (dereddened) intensities agree very well with those obtained by other authors. In particular, the agreement with the most recent study of PSM01 is better than 0.1 dex. As one should expect, the scatter increases towards fainter intensities.

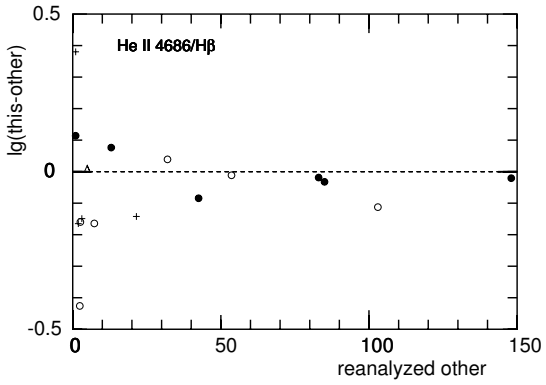

Fig. 3. The relative difference in intensity of the He II 4686Å line of our measurements compared to those of other works: Aller & Czyzak (1983, AC83, ×), Aller & Keyes (1987, AK87, +), Kingsburgh & Barlow (1994, KB94, ○), Cuisinier, Acker & Köppen (1996, CAK96, △), Cuisinier et al. (2000, CMAKS00, ▽), and Peña, Stasińska & Medina (2001, PSM01, •)

A comparison of the He I 5876Å lines (Fig.4) shows a good agreement with other studies. However, one notes a trend, in that our intensities tend to be larger than those of KB94, and to be smaller than those by PSM01 which is especially obvious in for larger intensities. Objects with

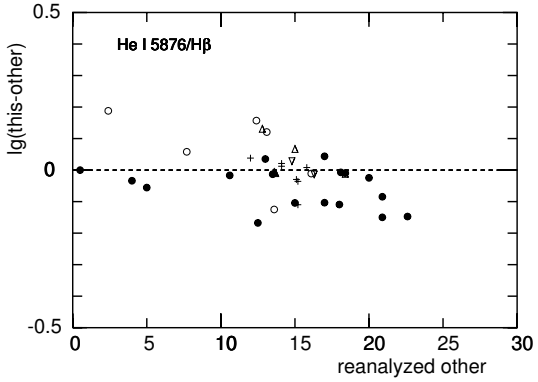

Fig. 4. The intensity of HeI 5876Å line compared to the value obtained by other works. Symbols are as in Fig. 3

large deviations are the [WO]s 002.4 + 05.8, 003.1 + 02.9, 017.9 − 04.8, 278.1 − 05.9, the [WC]s 006.8 + 04.1, 027.6 + 04.2, 048.7 + 01.9 and the *wels* 010.8 − 01.8. Since [WO] nebulae exhibit no stellar He I lines (cf. Acker & Neiner 2003), it is unlikely that our measurements are affected by confusion with the stellar spectrum. Furthermore, inspection of the other He I lines (4471, 6678, 7065, and 5015Å) shows that these line ratios are in good agreement with the intensity of the 5876 line.

The [O III] 4363 diagnostic line is of similar strength as the He I 5876 line. As shown in Fig. 5, our measurements are in good to fair agreement with the intensities obtained by the other studies. For intensities below 10 percent of Hβ the deviations with PSM01 are as large as a factor of two, in either direction. A similar finding is obtained for

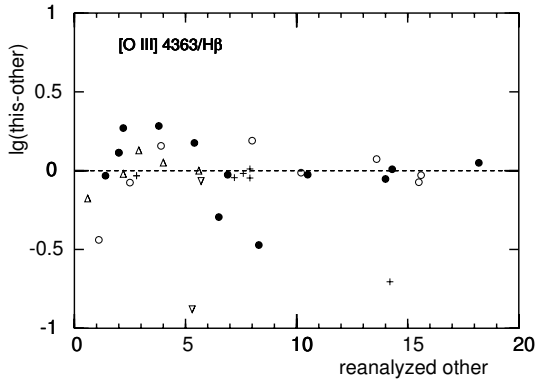

Fig. 5. The measured intensity of the [O III] 4363Å line compared to the values obtained by the other works. Symbols are as in Fig. 3

the [S II] 6717/31 Å doublet.

As a consequence of the difference in He I line intensities, our helium abundances differ slightly from the results of PSM01. This is addressed in more detail in Appendix 9. However, it does not affect the findings of this paper with respect to the evolutionary status of the [WR] PN.

2.1. A sample of 'normal' PNe

To compare the sample of [WR] nebulae with "normal" PN, we selected the objects from the following works: Although the image tube data from Aller & Czyzak (1983, hereafter AC83) and Aller & Keyes (1987, AK87) might be considered less reliable than present CCD data, such a suspicion is not too evident in individual comparisons. Moreover, these works constitute a large sample of the brighter PN, together with Kingsburgh & Barlow (1994, KB94). We include Cuisinier, Acker & Köppen (1996, CAK96) who focussed on objects high above the Galactic plane as well as the sample of Bulge nebulae by Cuisinier et al. (2000, CMAKS00). The inclusion of these samples does not constitute a major bias, since in our sample of [WR] objects there also is no selection against nebulae outside the disk.

To avoid possible influences by the different analysis methods employed by the other authors, we re-analyzed all the other spectra by our method using the same criteria. This includes using only the optical lines in the spectra of KB94. All together, this sample provides 167 objects with spectra of comparable quality which had been obtained for determinations of chemical compositions.

2.2. Comparison with other works

There are 3 nebulae in common with AC83, 7 with AK87, 8 with KB94, 6 with CAK96, 2 with CMAKS00, and in particular 17 with PSM01. This offers an opportunity to clarify to what extend the results from different studies are subject to differences in the measured line fluxes or to the adopted abundance determination methods. In Appendix 8 we compare the results obtained from reanalysis of the data by HOPPLA with the original values. The differences in the observational data are addressed in Appendix 9.

3. Plasma analysis of the nebular spectra

Extinction constants, electron temperatures and densities, and elemental abundances are determined with the computer programme HOPPLA (see Acker et al. 1991, and Köppen et al. 1991). The spectra are interpreted by the technique of plasma diagnostics, viz. assuming that all lines are produced in an isothermal gas at uniform density and ionization level. In the first step, the reddening correction, derivation of electron temperature and density, as well as the optical depth of the He I 3888 Å line (for self-absorption in the He I lines) are performed. These steps are repeated several times, until the values converge.

The excitation class (EC), absolute Hβ fluxes seen through the spectrograph aperture, extinction constants c, electron temperatures and densities for all selected 48 PN are compiled in Table 2. The last column gives an indication of the overall quality of the analysis. 'A' means that all diagnostic lines are present, 'B' that the density could not be reliably determined, and 'C' that the electron temperature could not be derived.

The extinction measure c is obtained from the decrement of all the observed Balmer lines relative to the one computed from Brocklehurst (1972) for case B. To find the optimum value, the error from each line is weighted with the square of the observed line flux. This weighting had been chosen to be able to deal also with rather noisy spectra; for the present data this suppresses the noise in the blue region of the spectrum, by given a strong weight to the Hα/Hβ ratio. In Fig. 6 we compare our values of the extinctions against the results found by other authors. For most of the objects we obtain good agreement with previous studies; yet for several nebulae rather discrepant values have been reported, most probably due to the difficulty to separate the nebular from the stellar emission lines. Notable exceptions are collected in Table 1.

Electron temperatures T_e are derived from line intensity ratios of [O III] (4959Å + 5007Å)/4363Å and [N II] (6548Å + 6584Å)/5755Å. We note that the high [N II] temperature in 337.4 + 01.6 is the consequence of its density to be close to the high density limit of the [S II] lines. Figure 7 shows the comparison of our values of the [O III] temperature for the objects common with other authors. There is an overall good agreement and no obvious systematic offset. In particular, we confirm the rather high temperature in 278.8 + 04.9 as found by PSM01.

Figure 8 shows the relation of [O III] and [N II] temperatures for the [WR] PN in comparison with the data for the non-WR PN. Save for the exception of 278.8+04.9, the PN with [WR] central stars follow the same relation between the temperatures as the normal PN, but they tend to have lower [O III] temperature. There is no difference between [WO], [WC], and *wels* nebulae. The distribution of objects in this diagram is very similar to that found by Górny et al. (2004) (their Fig. 2), with a strong concentration near 10^4 K. In our data there are fewer objects whose [N II] temperature exceeds the one from [O III].

Table 1. Nebulae whose extinctions found in this work and in the literature show strong differences. Other works are indicated by their abbreviations (e.g. KB94 for Kingsburgh & Barlow 1994) used in the References

PN G	this work	other works	
002.2 − 09.4	0.39	0.44 TASK92,	0.1 PSM01
004.9 + 04.9	1.46	1.46 TASK92,	1.0 PSM01
009.4 − 05.0	0.92	0.96 AK87,	0.6 PSM01
017.9 − 04.8	0.52	0.51 SK89,	1.30 TASK92
061.4 − 09.5	0.00	0.09 AC83,	0.27 KB94,
		0.45 CMB98,	0.23 PSM01
292.4 + 04.1	0.68	0.38 TASK92,	2.7: KB94
300.7 − 02.0	2.49	2.17 TASK92	
331.3 + 16.8	0.36	0.64 KB94	
358.3 − 21.6	0.18	0.33 AKF86	

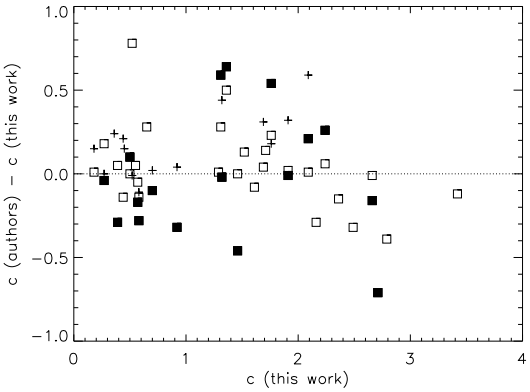

Fig. 6. The extinctions found in this work compared to other works for the same nebulae. Open squares refer to Acker & Neiner (2003) (from Crowther et al. 1998 and Tylenda et al. 1992), filled squares to PSM01, and plus-signs to AC83, Aller & Keyes (1980, 1987), Aller et al. (1981, 1986), Barker (1978), KB94, and Shaw & Kaler (1989)

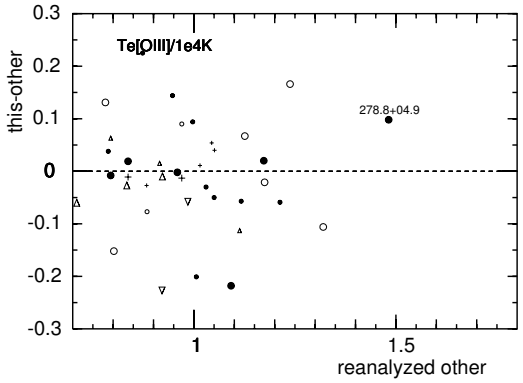

Fig. 7. Comparison of the [O III] electron temperatures derived in this work and determined by other authors for the same objects; symbols are the same as in Fig.3. Smaller symbols indicate that in the other work the values was marked as uncertain

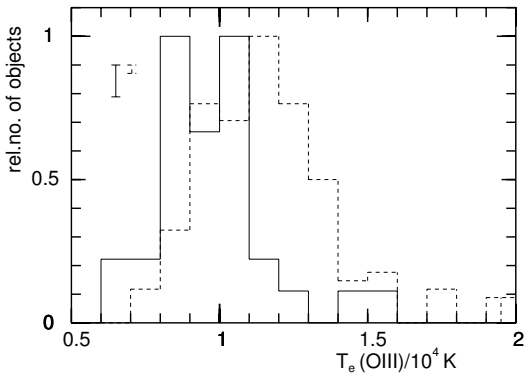

Fig. 9. Histograms of the [O III] electron temperature for the [WR] and *wels* objects (full line) and the non-WR objects (dashed). The vertical error bars indicate the contribution by a single object, the larger one refers to the [WR] objects

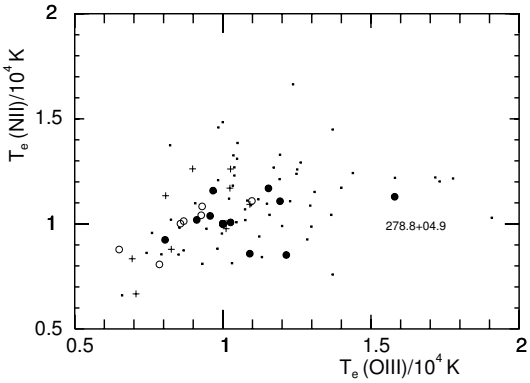

Fig. 8. Relation between electron temperatures from [O III] and [N II] line ratios for PN with central stars of types [WO] (filled circles), [WC] (open circles), *wels* (plusses), and any other (small dots)

The lower electron temperatures in the [WR] objects also show up clearly in the histogram (Fig. 9). The average temperature is 9730 ± 330 K from 33 [WR] and *wels* objects, significantly lower than 11680 ± 200 K from the 184 non-[WR] objects. Both distributions have similar dispersions: 1900 ± 230 K and 2620 ± 140 K, respectively.

Inspection of the temperatures and excitation classes shows a mild tendency for both [N II] and [O III] temperatures to increase with increasing excitation class, but no significant difference could be found in the behaviour of [WR] and non-WR PN. 278.8 + 04.9 remains exceptional in having one of the highest [O III] temperatures found among any PN.

Electron densities n_e are determined from the intensity ratios of the doublet [S II] 6717/6731Å. If the [S II] lines cannot be measured, we use the [Cl III] 5517/5537Å ratio (indicated by "C" in Table 2). In several nebulae the [S II] line ratio is close to the high-density limit. PNe whose density exceeds 20,000 cm^{-3} are marked by a "H" in Table 2 and this adopted value is used in further analysis.

4. Chemical compositions of the nebulae

With the electronic temperatures and densities obtained from the analysis of line ratios described above, the emissivities of all lines can be computed and thus from the observed dereddened intensities the ionic abundances relative to H^+ are deduced. Whenever both [N II] and [O III] electron temperatures are available, we use the [N II] temperature for the low ionization species (N^+, O^+, S^+, S^{++}) and the [O III] temperature for the higher species (O^{++}, Ne^{++}, Ar^{++},Ar^{3+}). To correct for unseen stages of ionization, the usual empirical correction factors (ICF) are applied (see Aller 1984). Table 3 presents the derived abundances of the 48 nebulae. All abundances are expressed in the usual logarithmic form of $12 + \lg(n(\mathrm{X})/n(\mathrm{H}))$.

For helium, the abundances of He^+ and He^{++} are derived from the He I and He II recombination lines. The emissivities of the He I lines are corrected for self-absorption and collisional excitation. In low excitation nebulae there could be present an appreciable amount of unobservable neutral helium. Therefore the He abundances in low excitation nebulae (EC 4 and less) are only lower limits and are marked with a colon in Table 3. For the sulphur ICF, we use the recipe of Samland et al. (1992), while for chlorine we apply a simple formula that gave a reasonable approximation to results from photoionization models:

$$\frac{\mathrm{Cl}}{\mathrm{H}} \approx \frac{\mathrm{Cl}^{++}}{\mathrm{H}^+} \left(\frac{\mathrm{He}}{\mathrm{He}^+}\right)^2$$

Table 2. Plasma parameters of the planetary nebulae of this sample. The spectral types are from Acker & Neiner (2003). Given are: excitation classes EC following Aller's (1956) system, Hβ fluxes in erg s^{-1} cm^{-2}, extinction constant c, electron temperatures from the [O III] and [N II] line ratios in 10^4 K, electron density from the [S II] line ratio in units of 1000 cm^{-3}. Values marked with 'A' are default values assumed in absence of the line ratio; densities marked with 'H' are lower limits because of the saturation of the [S II] ratio for high densities, densities marked with 'C' are from the [Cl III] lines

PN G	common name	Spec.Type	EC	lg(F(Hβ))	c	T(OIII)	T(NII)	n(SII)
000.4 − 01.9	M 2-20	WC5-6	4	−12.80	1.71	—	0.79	5.40
002.2 − 09.4	Cn 1-5	WO4pe	5	−11.75	0.42	0.87	—	4.82
002.4 + 05.8	NGC 6369	WO3	5	−13.50	1.91	0.80	0.92	1.74
003.1 + 02.9	Hb 4	WO3	6	−12.50	1.76	0.96	1.04	6.71
004.8 − 22.7	He 2-436	WC4	5	−12.39	0.55	1.00A	1.00A	12.92 C
004.9 + 04.9	M 1-25	WC4	4	−12.24	1.46	0.79	0.81	8.00
006.0 − 03.6	M 2-31	WC4	5	−12.50	1.29	0.93	1.08	5.31
006.4 + 02.0	M 1-31	wels	5	−12.73	2.00	—	0.99	11.70
006.8 + 04.1	M 3-15	WC4	5	−12.89	2.08	1.10	1.11	5.56
009.4 − 05.0	NGC 6629	wels	5	−12.16	0.92	0.86	—	2.13
010.8 − 01.8	NGC 6578	wels	5	−12.49	1.35	0.83	0.88	7.46
011.7 − 00.6	NGC 6567	wels	5	−11.47	0.70	1.09	1.09	10.46
011.9 + 04.2	M 1-32	WO4pe	4	−12.53	1.30	1.09	0.86	9.25
012.2 + 04.9	PM 1-188	WC10	< 2	−14.53	1.36	1.00A	1.00A	2.29
016.4 − 01.9	M 1-46	wels	< 2	−12.33	1.07	—	0.69	2.83
017.9 − 04.8	M 3-30	WO1	7	−14.07	0.52	1.00A	1.00A	3.40
019.4 − 05.3	M 1-61	wels	5	−11.74	1.71	0.93	—	16.41
019.7 − 04.5	M 1-60	WC4	5	−12.67	1.52	0.86	1.00	6.93
020.9 − 01.1	M 1-51	WO4pe	5	−13.92	3.37	—	0.88	7.73
027.6 + 04.2	M 2-43	WC7-8	4	−12.79	2.67	1.00A	1.00A	11.00 C
029.2 − 05.9	NGC 6751	WO4	5	−13.06	0.50	1.06	—	2.27
034.6 + 11.8	NGC 6572	wels	5	−10.73	0.30	1.02	1.17	17.41
038.2 + 12.0	Cn 3-1	wels	< 2	−11.33	0.44	—	0.75	6.90
048.7 + 01.9	He 2-429	WC4	4	−13.36	2.21	—	0.84	7.16
055.5 − 00.5	M 1-71	wels	5	−12.52	2.18	0.90	1.26	12.39
057.2 − 08.9	NGC 6879	wels	5	−11.70	0.42	1.03	1.26	4.16
061.4 − 09.5	NGC 6905	WO2	7	−12.84	0.00 A	1.15	1.17	0.53
068.3 − 02.7	He 2-459	WC9	< 2	−13.38	2.65	1.00A	1.00A	16.17
253.9 + 05.7	M 3-6	wels	5	−12.05	0.49	0.81	1.13	5.21
258.1 − 00.3	He 2-9	wels	4	−12.71	2.22	1.01	0.98	10.85
274.6 + 02.1	He 2-35	wels	5	−12.29	0.80	0.87	—	1.97 C
278.1 − 05.9	NGC 2867	WO2	7	−11.57	0.58	1.19	1.11	2.81
278.8 + 04.9	PB 6	WO1	7	−13.38	0.57	1.58	1.13	2.89
285.4 + 01.5	Pe 1-1	WO4	5	−12.72	2.16	0.97	1.16	18.31
291.3 − 26.2	Vo 1	WC10	< 2	−14.15	2.19	1.00A	1.00A	5.00 C
292.4 + 04.1	PB 8	WC5-6	6	−12.01	0.67	0.65	0.88	3.99
300.7 − 02.0	He 2-86	WC4	5	−12.62	2.49	0.87	1.01	11.90
307.2 − 03.4	NGC 5189	WO1	5	−13.33	0.44	1.21	0.85	0.48
327.1 − 02.2	He 2-142	WC9	< 2	−12.34	2.11	—	0.75	20.00 H
331.3 + 16.8	NGC 5873	wels	7	−11.56	0.37	1.40	—	5.19
336.2 − 06.9	PC 14	WO4	5	−12.16	0.65	0.91	1.02	3.05
337.4 + 01.6	Pe 1-7	WC9	< 2	−12.69	2.79	—	1.64	20.00 H
351.1 + 04.8	M 1-19	wels	4	−12.27	1.24	0.69	0.83	5.49
355.2 − 02.5	H 1-29	WC4	5	−12.81	1.61	0.93	1.04	7.30
355.9 − 04.2	M 1-30	wels	3	−12.24	1.01	0.71	0.67	4.93
356.7 − 04.8	H 1-41	wels	7	−12.67	0.65	1.01	1.00	1.17
357.1 + 03.6	M 3-7	wels	4	−12.80	1.83	—	0.78	4.67
358.3 − 21.6	IC 1297	WO3	7	−11.62	0.18	1.03	1.01	2.80

4.1. Elements synthesized in progenitor stars

Helium and nitrogen are elements that are produced in more massive progenitor stars of PN. Hence abundances of these elements is expected to be an indicator of the mass of the progenitor star. Comparing the histogram of helium abundances (Fig. 10), we find no evidence for any

Table 3. Elemental abundances for the nebulae. Uncertain values are marked with a colon.

PN G	Q	He	N	O	Ne	S	Ar	Cl
000.4 − 01.9	A	11.06 :	8.17	8.78	7.85	7.23	6.61 :	5.21 :
002.2 − 09.4	A	11.10	8.52	8.76	8.24	7.22	6.68	5.27 :
002.4 + 05.8	A	10.92 :	8.29	8.91	8.40	7.04	6.37 :	—
003.1 + 02.9	A	11.02	8.60	8.72	8.16	7.08	6.49	5.17 :
004.8 − 22.7	C	11.07 :	7.29 :	8.50 :	7.75 :	6.74 :	5.86 :	4.28 :
004.9 + 04.9	A	11.09 :	8.41	8.75	7.47	7.26	6.66	5.31 :
006.0 − 03.6	A	11.02	8.49	8.70	8.06	7.04	6.40	4.97 :
006.4 + 02.0	A	11.09 :	8.31	8.49	—	6.87	6.42 :	5.05
006.8 + 04.1	A	10.99 :	8.01	8.36	7.68	6.72	6.14 :	4.77 :
009.4 − 05.0	A	10.96	7.56	8.67	7.96	6.45	6.23 :	5.84
010.8 − 01.8	A	11.03	7.94	8.75	8.17	6.88	6.83	5.20
011.7 − 00.6	A	10.96	7.61	8.42	7.67	6.41	5.73	4.70
011.9 + 04.2	A	11.07 :	8.35	8.66	7.58	7.34	6.89	4.93 :
012.2 + 04.9	C	—	8.12 :	8.57 :	—	6.99 :	5.84 :	—
016.4 − 01.9	A	10.88	7.95	8.87	—	7.13	6.53 :	5.24 :
017.9 − 04.8	C	11.09 :	7.02 :	8.48 :	—	6.91 :	6.53 :	—
019.4 − 05.3	A	10.90	8.06	8.49	7.87	6.58	6.17	5.48 :
019.7 − 04.5	A	11.07	8.96	8.78	8.22	7.21	6.67	4.72 :
020.9 − 01.1	A	11.08 :	8.29	8.92	8.52	7.28	6.54 :	5.24 :
027.6 + 04.2	C	10.92 :	7.24 :	8.63 :	7.10 :	6.87 :	6.16 :	4.55 :
029.2 − 05.9	A	11.06 :	8.34	8.69	8.06	6.94	6.46 :	—
034.6 + 11.8	A	11.04	8.31	8.60	7.93	6.52	6.33	4.83
038.2 + 12.0	A	10.68	7.95	8.79	—	6.99	6.15	4.95 :
048.7 + 01.9	A	11.06 :	8.41	8.77	—	7.24	6.81	5.34 :
055.5 − 00.5	A	11.03 :	8.62	8.76	8.01	6.52	6.50	4.93
057.2 − 08.9	A	10.99	7.93	8.52	7.87	6.80	6.14	4.64 :
061.4 − 09.5	B	10.93 :	8.47	8.85	8.18	7.13	6.18	5.60 :
068.3 − 02.7	C	9.48 :	7.77 :	7.85 :	—	7.03 :	—	4.45 :
253.9 + 05.7	A	11.05	7.77	8.71	8.15	6.73	6.35	5.07 :
258.1 − 00.3	A	10.96 :	7.73	8.44	7.69	6.57	6.80	4.70 :
274.6 + 02.1	A	11.00	7.23	8.73	8.10	6.77	6.24	4.95 :
278.1 − 05.9	A	10.99	7.99	8.64	7.96	6.71	6.04	4.97 :
278.8 + 04.9	A	11.16	8.94	8.79	8.23	6.82	6.12	—
285.4 + 01.5	A	10.99 :	8.15	8.62	8.02	6.62	6.34	4.91
291.3 − 26.2	C	11.02 :	7.39 :	8.65 :	—	6.58 :	—	—
292.4 + 04.1	A	11.08	8.33	8.82	8.18	6.84	6.69	5.36
300.7 − 02.0	A	11.05 :	8.79	8.67	7.93	7.13	6.54	5.13 :
307.2 − 03.4	A	10.72 :	8.41	8.38	7.75	7.53	6.41	4.85 :
327.1 − 02.2	B	10.67 :	8.22 :	8.95 :	—	6.90 :	5.40 :	5.12 :
331.3 + 16.8	A	10.95	7.22	8.38	7.74	7.23 :	5.67 :	5.18
336.2 − 06.9	A	11.03	8.25	8.77	8.12	7.06	6.38	5.09 :
337.4 + 01.6	B	10.17 :	7.22 :	6.93 :	—	6.10 :	4.97 :	3.82 :
351.1 + 04.8	A	11.01 :	8.39	8.86	8.17	7.06	6.62 :	5.28 :
355.2 − 02.5	A	11.01 :	8.26	8.67	8.04	6.81	6.29	4.95 :
355.9 − 04.2	A	11.09	8.49	8.79	7.89	7.30	6.76	5.28 :
356.7 − 04.8	A	11.03	8.00	8.57	7.87	6.78	6.09	5.27
357.1 + 03.6	A	11.00	7.91	8.68	7.98	7.06	6.36 :	5.11 :
358.3 − 21.6	A	11.05	8.37	8.77	8.10	7.10	6.27	5.37

significant difference between 42 WRPN and 177 "normal" PN. The respective averages of 11.022 ± 0.009 and 11.021 ± 0.006 are the same, as are the dispersions: $\sigma = 0.061 \pm 0.007$ and $\sigma = 0.082 \pm 0.004$.

Likewise, the relation between helium abundance and the N/O abundance ratio exhibits no clear difference between the two types of nebulae. Neither is obvious any difference between objects with [WO], [WC], or *wels* central stars, as depicted in Fig. 11. Two objects fullfill the criterion of Peimbert & Torres-Peimbert (1983) for Type I nebulae: the [WO] types $002.2 - 09.4$ and $278.8 + 04.9$, and with the *wels* $006.4 + 02.0$ doing nearly so.

The average helium abundances (Table 4) for all types are solar without any significant differences. The nitrogen

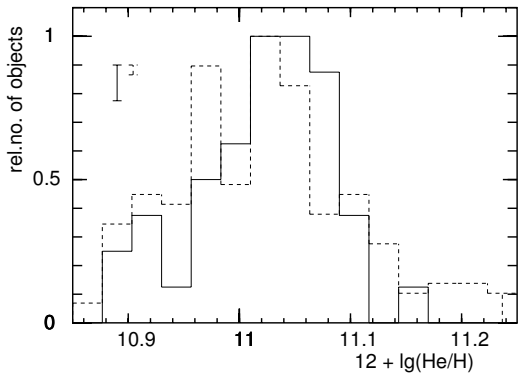

Fig. 10. Distribution of helium abundances among [WR] and *wels* PN (full line) and "normal" PN (dashed line). The vertical error bars indicate the contribution by a single object, the larger one referring to the [WR] objects

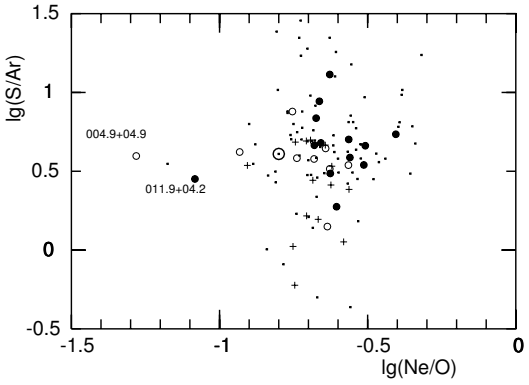

Fig. 12. Relation between the abundance ratios Ne/O and S/Ar. The symbols are as in Fig. 8. The solar symbol indicates solar values (lg(Ne/O) = −0.80 and lg(S/Ar) = 0.61)

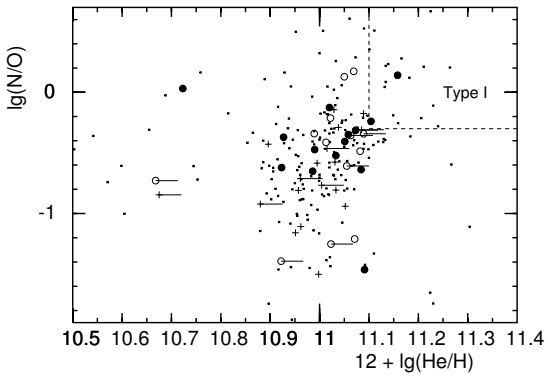

Fig. 11. Relation between helium abundances and N/O abundance ratios for WR and "normal" PN. The symbols are as in Fig. 8. Short bars indicate a lower limit to the He abundance in WRPN of excitation class below 5

abundance in [WC] and [WO] is somewhat enhanced with respect to the Sun, but *wels* and "normal" PN have solar values. The N/O abundance ratio found in both [WC] and [WO] type nebulae is about thrice solar, but in non-WR nebulae it is not more than twice solar. The *wels* objects have nearly a solar ratio. One also notes that the helium abundance is somewhat lower, by about twice the standard error. It thus is tempting to identify *wels* nebulae as coming from less massive progenitor stars than the other types of PN.

4.2. The other elements

Oxygen, neon, sulphur, and argon are synthesized in massive stars, and their abundances are not altered by the nucleosynthesis in the PN progenitor stars. The average oxygen abundances, presented in Table 4, among [WO], *wels*, and "normal" PN are slightly below the solar value, but [WC] nebulae have still lower values (about a factor 2 below the average PN). This pattern is also seen with neon: the [WC] objects are about 0.2 dex below the other PN, among which no significant difference is ascertained. Sulphur and argon in PN of all types are lower than in the Sun; this reflects the limitation of the empirical ICFs. In interpreting the lower abundances found among the [WC] objects, one has to keep in mind that these objects tend to be dense nebulae of low excitation, i.e. with spectra less favourable for plasma diagnostics. But if one regards 006.0 − 03.6 or 292.4 + 04.1, as examples of high excitation spectra with all diagnostic lines, the derived abundances are very close to those of the Sun. Therefore, the chemical compositions of planetary nebulae with central stars of types [WC], [WO], and *wels* do not differ from those of nebulae with "normal" central star, and are nearly solar.

The abundance ratios Ne/O and S/Ar, shown in Fig. 12, of either type of PN are rather close to the ratios found in the Sun. Some slight differences can be noted, but since the ICF of Ar depends on S, whose ICF is based on O, it is rather likely that e.g. the concentration of [WC] near lg(S/Ar) = 0.7 with a large dispersion in Ne/O reflects more the analysis method than genuine chemical differences. There are two remarkable outliers, 004.9 + 04.9 (one of the three nuclei of [WC 5-6] type) and 011.9 + 04.2 (one of the four nuclei of type [WO 4p] which show very high velocity winds), which also stand out in diagrams of the other combinations of abundance ratios; neither object shows any obvious flaw in the observational material or analysis.

PSM01 had found unusually low Ne/O abundance ratios in 004.9 + 04.9 (0.00343) and 011.9 + 04.2 (0.00371). Our values (0.052 and 0.083) are higher, but still substantially lower than the solar value of 0.16. The other non-WR object is 325.4 − 04.0 observed by Kingsburgh & Barlow (1994).

Table 4. Average abundances for the PN of each type, along with the standard error. Only values without a colon in Table 3 from class 'A' analyses are taken into account; helium in [WC] PN comes from only 3 objects. The values for the non-WR sample comes from our reanalysis of the published data

Element	[WC]	[WO]	*wels*	non-WR	solar
He	(11.06 ± 0.03)	11.06 ± 0.06	10.99 ± 0.05	11.03 ± 0.08	11.00
N	8.43 ± 0.28	8.37 ± 0.23	7.94 ± 0.38	8.13 ± 0.55	8.07
O	8.70 ± 0.13	8.72 ± 0.14	8.64 ± 0.15	8.57 ± 0.26	8.83
Ne	7.93 ± 0.24	8.10 ± 0.25	7.94 ± 0.16	7.92 ± 0.30	8.03
S	7.05 ± 0.20	7.06 ± 0.25	6.79 ± 0.25	6.78 ± 0.30	7.19
Ar	6.58 ± 0.17	6.40 ± 0.25	6.34 ± 0.32	6.22 ± 0.28	6.56
N/O	-0.27 ± 0.25	-0.35 ± 0.25	-0.70 ± 0.35	-0.44 ± 0.48	-0.76

5. Other global relations

In the diagnostic diagram of the intensity ratios Hα/[N II] and Hα/[S II] (Fig. 13, after Cantó 1981 and Corradi et al. 1997), the nebulae of our sample cover the region occupied by planetary nebulae. Except for some preference of the [WO] objects to do not extend to high Hα/[S II] and Hα/[N II] ratios, no specific region for [WR] nebulae can be distinguished.

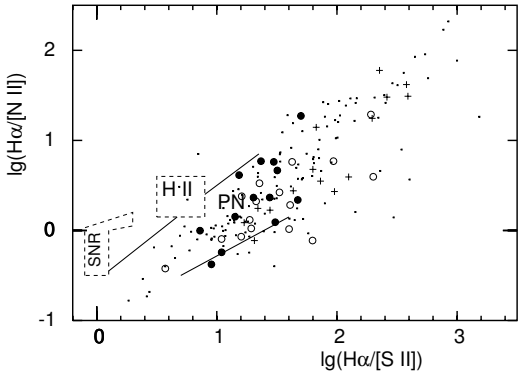

Fig. 13. The intensity ratios Hα/[N II] and Hα/[S II] of our objects, in relation to the regions identified by Cantó (1981). The symbols are as in Fig. 8.

The diagram of dereddened Hβ flux and angular diameter allows some inferences on the number of ionizing photons from the central star: In an ionization bounded Strömgren sphere of radius R, the dereddened Hβ flux at a distance d depends on the number of ionizing photons as

$$\mathcal{N}_{LyC} = \frac{4\pi}{3}\alpha_B R^3 n^2 = \frac{\alpha_B}{\alpha_{\rm eff}} \cdot 4\pi d^2 \cdot F_0(\mathrm{H}\beta) \qquad (1)$$

with the coefficients α_B for all recombinations to excited levels and $\alpha_{/rmeff}$ for leading to the emission of Hβ photons. Using the relation $R/d = \sin(D) = D$ between angular diametre D and R, one obtains

$$F_0 d^2 \propto F_0/D^2 \cdot \mathcal{N}_{LyC}^{2/3} \cdot n^{-4/3} \qquad (2)$$

and demanding that the ionized mass $M_{\rm ion} = 4\pi n m R^3/3$ remains constant, one gets

$$F_0 \propto D^2 \cdot \mathcal{N}_{LyC}^{5/3} \cdot M_{\rm ion}^{-4/3} \qquad (3)$$

Taking the optical diameters from the catalog of Acker et al. (1992), we find in Fig. 14 that [WC] nebulae tend to be small (below 20 arcsec) while nebulae with [WO] type central stars do not appear to be different from "normal" PN. Such a behaviour ties in well with the notion that [WC] objects are young and compact nebulae. The *wels* also tend to be small (below 20 arcsec). The range in the number of ionizing photons is the same in all four groups. One also has to keep in mind that these numbers depend on the ionized mass of the nebula, which might vary among the types.

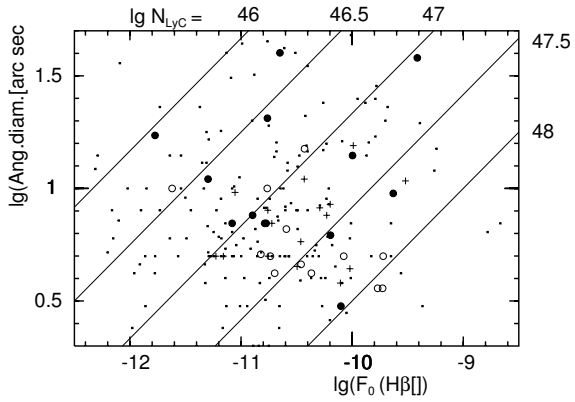

Fig. 14. Dereddened Hβ fluxes and angular diameters of nebulae with central stars of the various types, denoted by the same symbols as in Fig. 8. The lines of constant number of ionizing photons (in photons s^{-1}) are computed for ionization bounded nebulae of 0.25 solar masses

As the mid-infrared colours from the satellite IRAS are indicative of the temperature of the dust shell surrounding the nebula, we inspect the two-colour diagrams (Figs. 15 and 16) for relations with the spectral type of the central star. However, in neither diagram the PN

with [WR]-type central stars show a behaviour that is markedly different from the sample of "normal" nebulae. Also, the *wels* objects do not exhibit any clear characteristics. All objects have infrared flux distributions similar to black bodies of temperatures between about 100 to 200 K. One object stands out, as already noticed by Acker et al. (1996a): 336.2 − 06.9 is brighter both in the 12 and 100μm bands, relative to the 25 and 60μm bands, than a blackbody.

The objects in our sample are distributed in the same region as the WRPN in Figs. 8 and 9 of Górny et al. (2001). These authors also showed that WR and non-WRPN are distributed very similarly in the IRAS two-colour diagrams (their Fig. 5), which indicates that the nebulae expand in a similar way and thus the dust heating drops accordingly.

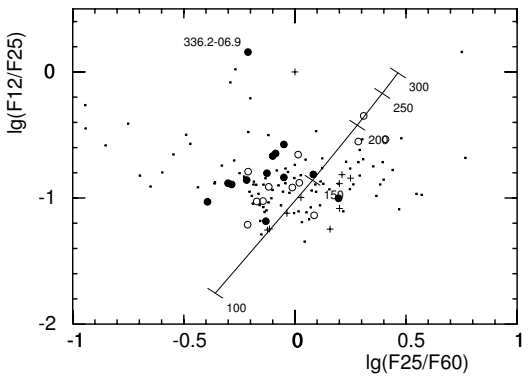

Fig. 15. Two-colour diagram of IRAS fluxes at 12, 25, and 60 μm. Symbols have the same meaning as in Fig. 8. Only high quality data is included. The line with ticks indicates the colours of black-body spectra between 100 and 300 K

From the DENIS database at CDS we extracted the infrared colours for our objects (10 [WO], 14 [WC], 13 *wels*, and 94 non-WR nebulae). In the two colour diagram (Fig. 17) of the I(0.82μm), J(1.25μm) and K(2.15μm) bands, most nebulae of all types cluster near colour temperatures of 4000 K. While none of the [WO] objects is not found elsewhere, several [WC] nebulae are found at high $(J\text{-}K)_0$ colour indices: 004.8 − 22.7, 012.2 + 04.9, 027.6 + 04.2, 291.3 − 26.2, and 327.1 − 02.2. Likewise, two *wels* are found with high $(I\text{-}J)_0$ values: 010.8−01.8 and 357.1+03.6. Inspection of the DENIS data reveals that none of these objects has magnitude errors in excess of the other objects. Neither do we find correlations with other nebular properties, such as Hβ flux, extinction, or angular diametre.

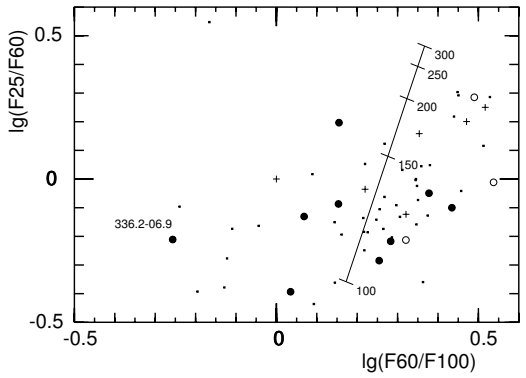

Fig. 16. Same as Fig. 15, but for the fluxes at 25, 60, and 100 μm

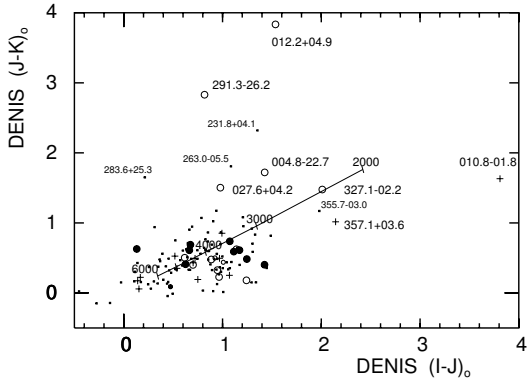

Fig. 17. The two-colour diagram of I-J vs J-K from DENIS data. The line with ticks indicates colours from blackbody with temperatures from 3000 to 6000 K. The symbols are as in Fig. 8

6. Relations between central star and nebula

To explore the possibilty of an evolutionary sequence from [WC 11] to [WO 1], we investigate the nebular properties as a function of the spectral type of their central stars. Since the excitation class is a measure of the temperature of the ionizing source, it is expected to be linked to the temperature of the central star. Figure 18 indicates a clear relation between spectral type and excitation class, in the sense that [WC] central stars are found in low excitation nebluae, while the early [WO] stars are surrounded by nebulae of highest excitation. The *wels* central stars are found in objects of any level of excitation. Given the small sample, we regard the large number with EC = 5 an observational selection effect.

This is also evident in the electron temperatures, depicted in Fig. 19. Unfortunately, there are no measure-

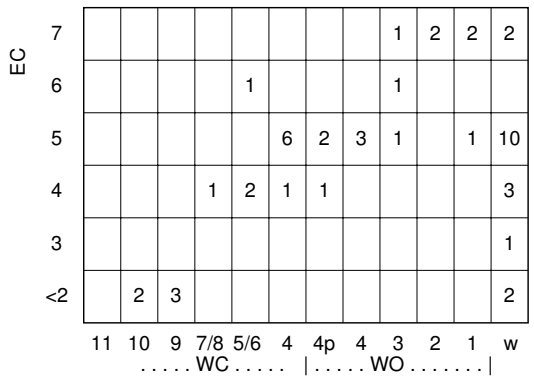

Fig. 18. Distribution of nebulae among central star spectral types and excitation class of the nebula. The column marked 'w' refers to *wels* objects

ments of the [O III] temperature in the low excitation nebulae, and the few reliable [N II] temperatures do not allow to follow this correlation among these types of objects.

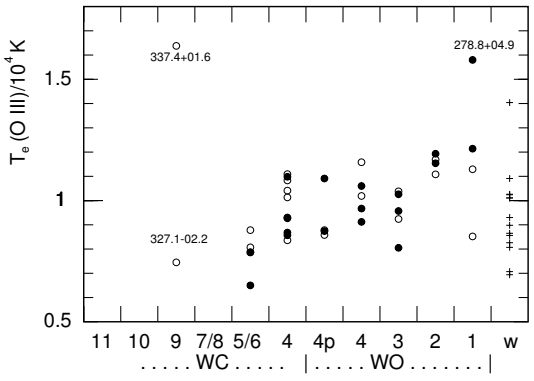

Fig. 19. Relation between spectral type and electron temperature from [O III] (filled circles) and from [N II] (open circles). *wels* are marked by a cross

Fig. 20 shows that the electron density decreases along the sequence from cooler [WC 10] to hot [WO 1]. This ties in well with the notion of an evolutionary sequence: as the density decreases due to the nebular expansion, the central star becomes hotter. In contrast, the *wels* objects display a wide range of densities, and cannot be incorporated into this sequence.

All these results support an evolutionary sequence from [WC 11] central stars which are cool and surrounded by dense, low excitation nebulae towards hot [WO 1] stars with low density, high excitation nebulae.

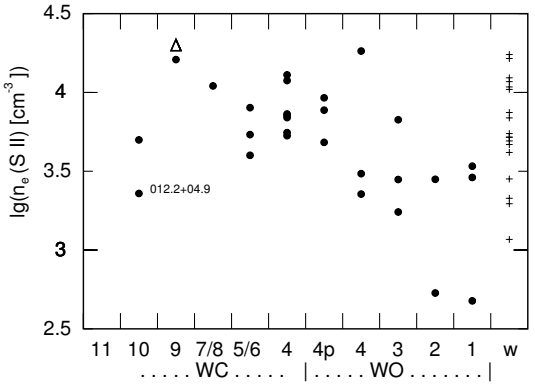

Fig. 20. Relation between spectral types and electron density from [S II]. "Δ" are the limit of density determination (marked 20.00H in table 2). *wels* are marked by a cross

The *wels* objects evidently belong to a different class of planetaries which do not appear to be evolutionarily related to the [WR] type nebulae.

7. Conclusion

Nebular spectra of 48 PN around central stars of [WR] and *wels* spectral type are analyzed for plasma properties and chemical compositions. Comparison of the results for [WC], [WO] and *wels* objects with the properties of "normal" non-WR type objects confirm that the nebulae of either group are very similar:

- they remain indistinguishable in Canto's diagnostic diagram
- the relation of electron temperatures from [N II] and [O III] lines show the same trend and range
- the average [O III] temperature in WRPN and *wels* objects is about 3000 K lower than in non-WR nebulae
- they have the same average helium abundances, and abundance distribution. *wels* have slightly lower helium abundances
- the nitrogen abundances in [WC] and [WO] nebulae are somewhat enhanced with respect to the Sun, while *wels* and non-WR PN have solar values
- the N/O abundance ratio in both [WC] and [WO] PN is about thrice solar, somewhat higher than in non-WR (less than twice solar). But *wels* objects have a much lower ratio, of nearly solar value.
- O, Ne, S, Ar abundances are nearly solar in all groups.
- [WC] and *wels* nebulae tend to be smaller than [WO] and non-WR objects
- the number of ionizing photons covers the same range and has the same average value
- all groups have very similar properties in the IRAS and DENIS colours
- in the DENIS two-colour diagram some [WC]s are found at high $(J\text{-}K)_0$ values while two *wels* have high $(I\text{-}J)_0$ colour indices.

With respect to the central star's spectral type, some clear trends are present: From [WC 11] to [WO 1],

- the excitation class rises, hence the temperature of the star's ionizing spectrum
- the electron temperature rises
- the electron density decreases

as one would expect for an evolutionary sequence from late to early spectra type, as the star heats up and the nebula expands. The *wels* nebulae have properties that cover a wide range, and they evidently belong to a separate subclass of PN, and do not appear to be evolutionarily related to the [WR] type nebulae.

Thus our results corroborate the evolutionary sequence from [WC 11] central stars which are cool and surrounded by dense, low excitation nebulae towards hot [WO 1] stars with low density, high excitation nebulae with embedded cooler dust. On the other hand, there is no evidence for the *wels* being linked by evolution to the [WR] PN. Rather they seem to constitute a separate class of objects with a variety of nebular properties. Their lower N/O ratio and the hint of a lower He/H abundance suggests that they might have formed from less massive progenitor stars than the other PN.

Acknowledgements. We thank Sophie Durand for a first measurement of the majority of the spectra. We wish to express our thanks to the referee for detailed comments and suggestions.

References

Acker A., Neiner C., 2003, A&A 403, 659 (AN03)
Acker A., Górny S.K., Cuisinier F., 1996a, A&A 305, 944
Acker A., Köppen J., Stenholm B., Raytchev, B., 1991, A&AS 89, 237
Acker A., Samland M., Köppen J., Stenholm B., 1989, ESO Messenger 58, 44
Acker A., Ochsenbein F., Stenholm B., Tylenda R., Marcout J., Schohn C., 1992, Strasbourg-ESO Catalogue of Galactic Planetary Nebulae (SECGPN), ESO, Garching
Acker A., Marcout J., Ochsenbein F., 1996b, First Supplement to the SECGPN, Observatoire de Strasbourg.
Aller L.H., 1956, Gaseous Nebulae, The international Astrophysics Series, vol. III, Chapman & Hall, London
Aller L.H., Czyzak S.J., 1983, ApJ 51, 211 (AC83)
Aller L.H., Keyes C.D., 1980, Ap&SS 72, 203 (AK80)
Aller L.H., Keyes C.D., 1987, ApJ Suppl. 65, 405 (AK87)
Aller L.H., Keyes C.D., Feibelman W., 1986, ApJ 311, 930 (AKF86)
Barker T., 1978, ApJ 219, 914
Berrington K.A., Kingston A.E., 1988, J.Phys.B 20, 6331
Brocklehurst M., 1972, MNRAS 157, 211
Cantó J., 1981, in *Investigating the Universe*, Reidel, Dordrecht, p.95
Corradi R.L.M., Villaver E., Mampaso A., Perinotto M., 1997, A&A 324, 276
Crowther P.A., De Marco O., Barlow M.J., 1998, MNRAS 296, 367 (CMB98)
Cuisinier F., Acker A., Köppen J., 1996, A&A 307, 215 (CAK96)
Cuisinier F., Maciel W.J., Acker A., Köppen J., Stenholm B., 2000, A&A (CMAKS00)
DENIS database at http://cdsweb.u-strasbg.fr/denis.html
Górny S.K., Stasińska G., 1995, A&A 303, 893
Górny S.K., Stasińska G., Szczerba R., Tylenda R., 2001, A&A 377,1007
Górny S.K., Stasińska G., Escudero A.V., Costa R.D.D., 2004, A&A 427, 231
Górny S.K., Tylenda R., 2000, A&A 362, 1008
Kingsburgh R.L., Barlow M.J., 1994, MNRAS 271, 257 (KB94)
Köppen J., Acker A., Stenholm B.,1991, A&A 248, 197
Mendoza C., 1983, IAU Symp. 103, 143
Peimbert M., Torres-Peimbert S., 1983, IAU Symp. 103 , 233
Peña M., Stasińska G., Medina S., 2001, A&A 367, 983 (PSM01)
Samland M., Köppen J., Acker A., Stenholm B., 1992, A&A 264, 184
Shaw A.R., Kaler J.B., 1989, ApJS, 69, 495 (SK89)
Tylenda R., Acker A., Stenholm B., Köppen J., 1992, A&AS 95, 377 (TASK92)
Tylenda R., Acker A., Stenholm B., 1993, A&AS 102, 595

8. Comparison of the methods

We reanalyzed with HOPPLA the dereddened line intensities of the objects in the other works and compare the plasma parameters and abundances with the authors' original values (except for CAK96 and CMAKS00 who also use HOPPLA).

Since both HOPPLA and PSM01 use nearly the same atomic data, and use rather similar strategies, the reanalysis of their data gives almost identical results: both [O III] and [N II] electron temperatures are retrieved within 100 K (i.e. within the 3 decimal places of the authors' data), and the [S II] densities are within 0.05 dex. As shown in Fig. 21, the helium abundances mostly agree within 0.01 dex; however, for several high excitation objects ($017.9-04.8, 061.4-09.5, 144.5+06.5, 161.2-14.8$, $189.1+19.8$, $243.3-01.0$, $278.1-05.9$, $278.8+04.9$, $286.3+02.8$) HOPPLA yields a smaller value, by as much as 0.06 dex. None of the objects shows discrepancies in electron density or temperature; however, in $061.4-09.5$ and $278.1-05.9$ the He I intensity is given as a single digit only (4 and 5), which could mean an uncertainty of as much as 20 percent. Another exception is $356.2-04.4$ for which a higher He abundance is found (by 0.08 dex). The origin for this discrepancy could not be found. The oxygen abundances (Fig. 22) are recovered within 0.1 dex, with the exceptions of $061.4-09.5$, $161.2-14.8$, $189.1+19.8$, $243.3-01.0$, $278.8+04.9$, and $286.3+02.8$ which have values as much as 0.2 dex higher than in PSM01. The origin is that in these high excitation objects the oxygen ICF depends on the (high) He^{++}/He ratio which propagates and amplifies the deviation found in the He abundances. The maximum deviation in the N/O abundance ratio (Fig. 23) is 0.05 dex in $004.9+04.9$. We conclude that both methods give nearly identical results.

We refrain from showing for the other works the plots of comparing original and re-derived values for all quantities, but present the essential results in Table 5 in numer-

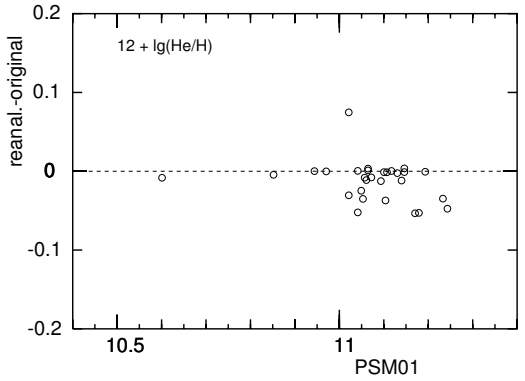

Fig. 21. The helium abundances of the PN observed by PSM01 compared to the values found by HOPPLA from the same data

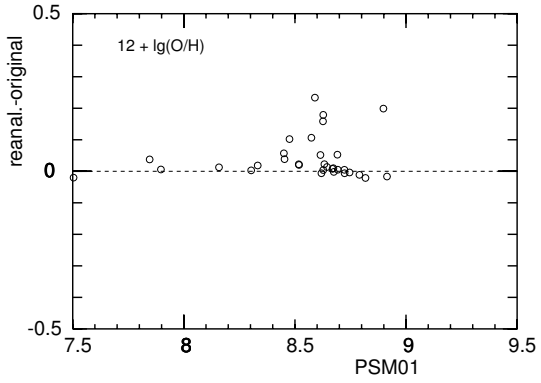

Fig. 22. The oxygen abundances of the PN observed by PSM01 compared to the values found by HOPPLA from the same data

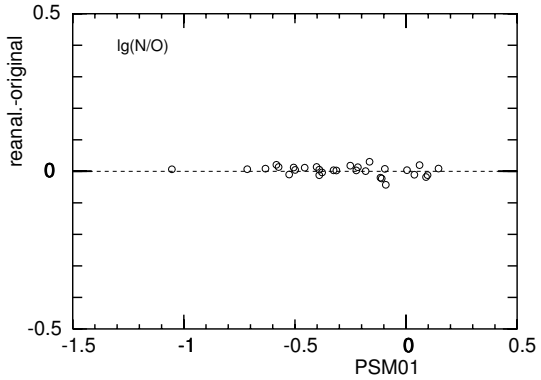

Fig. 23. The N/O abundance ratios of the PN observed by PSM01 compared to the values found by HOPPLA from the same data

ical form. We summarize the inspection of the plots of key quantities:

- KB94 include lines from the range 1200–3000A . Whether or not these lines are included in the analysis, has rather little impact, but in all plots we show only the results based on the optical lines. The [O III] temperature is recovered within 300 K, with several outliers which cause a non-zero mean and a large dispersion. The [N II] temperature shows a substantially larger dispersion, but with all deviations being within 1000 K; the majority of the objects give higher temperatures, causing a substantial offset. Electron densities are recovered by 0.1 dex, with seven exceptions. Plasma parameters can be obtained from the published spectra for 53 objects. Helium abundances are within 0.05 dex; three objects have lower abundances and two give higher values. The oxygen abundances show a strong scatter up to 0.4 dex without significant offset. The deviations in the N/O ratio are as large as 0.5 dex, with a clear tendency for HOPPLA getting larger values.
- the data of AC83 and AK87 display a similar behaviour: the temperatures (composed from several diagnostic ratios) are within about 1000 K of the [O III] temperatures in the reanalysis, with 3 outliers. Electron densities show a strong scatter as well as a systematic offset when compared with our values from [S II], because the published values are based on averages from different diagnostic line ratios. The helium abundances are systematically lower (by about 0.05 dex) than in the reanalysis, with a scatter of the same magnitude. This offset is due to our inclusion of the corrections of the He I emissivities for collisional excitation based on Berrington & Kingston (1988). Oxygen abundances show significant scatter but without any offset. The N/O ratio has strong dispersion with little offset.

Often the reason for one object to show a strong deviation in the results can be traced to some particular cause, such as a diagnostic line ratio being at or close to the limit of its sensitivity, resulting in a propagation of this error to other quantities. It would go beyond the aims of this paper to discuss these objects in detail, and thus trace in even more detail the origins of the differences found.

9. Comparison of the observational data

For the objects that we have in common with other works, we compare the results from the reanalysis with HOPPLA of their spectra with the present work. This reflects the differences in the measured intensities.

In Fig. 24 we compare our He/H abundances with the other studies. One notes a rather clear trend that we get lower helium abundances from our own data than from the the data of PSM01, especially for higher abundances. The results from the other data also are in line with this trend, although the fewer numbers do not allow to make a firm conclusion. As shown in Fig. 4, such a trend is already present in the intensities of the He I 5876Å line.

Table 5. Results of the reanalysis of PN spectra from previous studies using the HOPPLA code. The averages and the dispersions are given for the differences of the original values and our results. Default values used by HOPPLA in the absence of diagnostic lines or in the high density limit are not taken into account. Note that the electron temperatures and densities given by AC83 and AK87 are the values adopted from combining different diagnostic line ratios. The number of objects in each sample refers to those with helium abundances. For KB94 we also show the results based on the optical lines only (3700 ... 8000Å)

No.objects	AC83 18		AK87 42		KB94 52		KB94 (opt.) 52		PSM01 31	
	mean	disp.	mean	disp.	mean	disp.	mean	disp.	mean	disp.
T([OIII])	(−260)	(370)	(70)	(410)	−120	230	−180	220	20	60
T([NII])	—	—	—	—	−480	430	−580	320	10	100
lg(n[SII])	(0.073)	(0.155)	(−0.060)	(0.198)	−0.003	0.109	−0.003	0.109	0.005	0.022
He/H	0.039	0.024	0.037	0.033	0.010	0.028	0.004	0.025	0.011	0.024
O/H	0.004	0.212	0.033	0.145	−0.041	0.134	−0.009	0.115	−0.040	0.065
N/O	−0.102	0.212	0.014	0.184	−0.120	0.187	−0.092	0.144	−0.002	0.015

However, if one compares the reanalyzed data of PSM01 with the other works, another clear correlation is found, as depicted in Fig. 24. Again, this is reflected in PSM01 getting higher He I intensities for the stronger lines than by previous studies (Fig. 26).

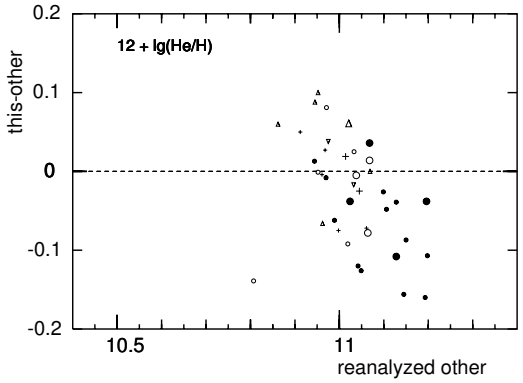

Fig. 24. Comparison of the helium abundances found in this work with the values obtained by reanalysis of the data from the other works. The symbols are the same as in Fig.3; smaller symbols denote those objects which HOPPLA assumed default values for the electron temperatures or density

With the other elements, no such clear trend is found, partially because the scatter is substantially larger. We summarize the results as average and dispersion of the deviations found: Table 6 gives the comparison between our data and the reanalysis of the PSM01 data. The plasma parameters do not show a systematic offset, except for the [N II] temperatures, but a large scatter, which indicates differences in S/N ratio which affect the faint lines. Neither O/H nor N/O have significant offsets, but appreciable scatter, part of which comes from the electron temperature differences. As already seen in Fig.7, the scatter in the [O III] electron temperatures is much larger than the differences due to the analysis methods. If we compare

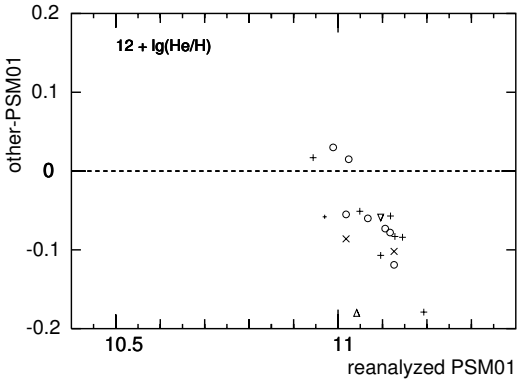

Fig. 25. Similar to Fig. 24, but comparing the reanalyzed PSM01 data with the reanalyzed data of AC83, AK87, KB94, CAK96, and CMAKS00, using the same symbols

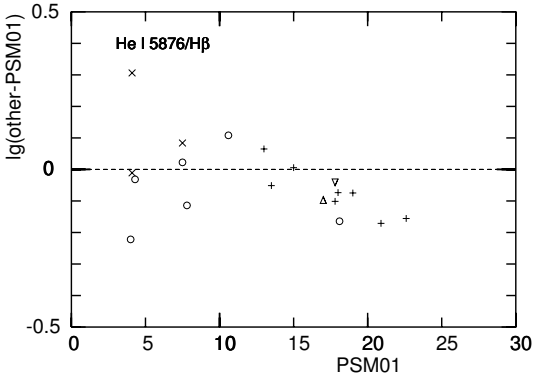

Fig. 26. Similar to Fig. 4, but comparing the PSM01 data with the data of AC83, AK87, KB94, CAK96, and CMAKS00, using the same symbols

the reanalysed PSM01 data with earlier data of the same objects, we find similar results; however, the discrepances

Table 6. The means and dispersions of the differences between the reanalyzed PSM01 data and this work, along with the formal bars. For the line intensities, the differences of $\lg(I/I(\mathrm{H}\beta))$ are used.

	mean	disp.	No.
T([OIII])	-10 ± 290	1130 ± 210	15
T([NII])	840 ± 330	1100 ± 240	11
lg(n[SII])	-0.142 ± 0.109	0.464 ± 0.077	18
lg(He/H)	0.053 ± 0.019	0.078 ± 0.013	17
lg(O/H)	-0.170 ± 0.151	0.623 ± 0.107	17
lg(N/O)	0.193 ± 0.106	0.439 ± 0.075	17
[O III] 5007	0.026 ± 0.019	0.080 ± 0.014	17
He II 4686	-0.091 ± 0.082	0.218 ± 0.058	7
He I 5876	0.056 ± 0.015	0.064 ± 0.011	17
[O III] 4363	-0.009 ± 0.056	0.201 ± 0.039	13
[S II] 6725	0.047 ± 0.037	0.154 ± 0.026	17

in the line intensities are stronger, as can be seen from Fig. 26.

In the quest to identify the origin of the deviation of the helium abundances derived by us and PSM01, the only clear trend is found to exist between this deviation and the absolute Hβ flux, as presented in Fig. 27. We note that the results from the other works are in line with the results of this work, in that large negative differences are found in faint objects. Because of the larger number of objects in common, this trend is more evident with our data.

Comparing the differences in the intensities of the He I 5876Å line from the corresponding works (Fig 28), one notes that for fainter nebulae the intensities from PSM01 tend to be smaller than in the other works, including our own. Inspection of the [S II] 6725Å and [O III] 4363Å lines, which are of comparable intensity, does not reveal a trend as clear as seen in the He I line.

We conclude that there exists a small but systematic difference in the helium abundances between our work and PSM01, in that the nebular He I lines in fainter objects have been either underestimated by us (and the other works) or overestimated by PSM01. Since the observational conditions are quite similar, yielding spectra of the same signal-to-noise ratio, we cannot determine the reason with certainty. Because a thorough reanalysis of our data did not reveal a possible underestimation of He I 5876Å fluxes, and the values are found to be in good agreement with the other He I lines, we tend to prefer our results.

This difference is larger than the differences due to the analysis methods and larger than uncertainties in atomic data, and thus it is somewhat annoying; however, it is not large enough to affect the findings on the status of WRPN.

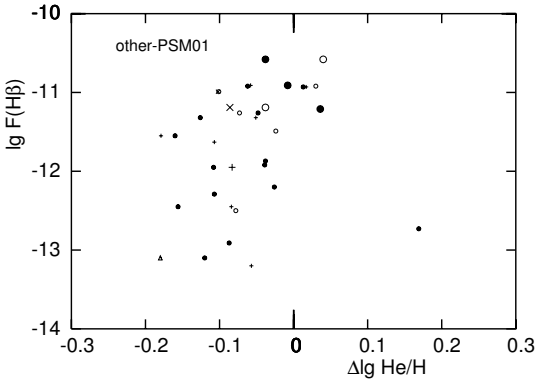

Fig. 27. Relation of the difference between helium abundances from the reanalyses of the data of AC83 ($\times$), AK87(+), KB94($\circ$), CAKS96 ($\triangle$), and this work ($\bullet$) with those from PSM01. Smaller symbols indicate nebulae where default values for electron temperature or density had to be assumed by HOPPLA.

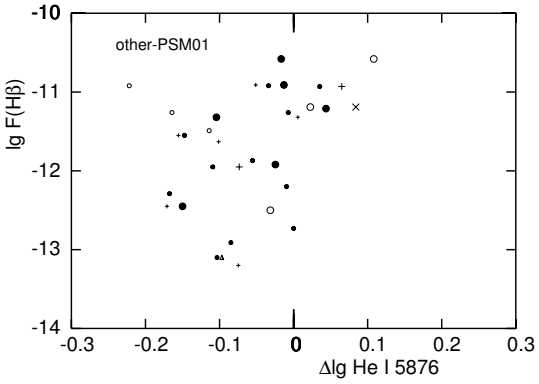

Fig. 28. Similar to Fig. 27, but for the intensity of the He I 5876 line.